3-D ray-tracing: Application to tomography

Jean Luc Guiziou

ABSTRACT

A fast ray-tracing algorithm based on continuation techniques enables us to model the traveltime of seismic rays which propagate through a three-dimensional layered medium. The algorithm is designed to handle many seismic lines spread on the surface of the earth arbitrarily. This ray-tracing is applied to a tomographic procedure so as to recover a 3-D layered image of the subsurface. The analytical link between the ray-tracing algorithm and the non-linear inversion algorithm leads to a computationally efficient tomographic scheme. A few synthetic examples demonstrate the method's ability to provide a reliable image of the earth.

INTRODUCTION

Processing methods in the two-dimensional space domain have been and still are heavily investigated. Even if there remain a lot of issues in two dimensions, geophysicists tend to extend more and more their data analysis methods to three dimensions. The major effect of this extension is an impressive increase in computational cost and until recently this cost was prohibitive, except perhaps for ray-tracing methods which were already used in the early seventies (e.g. Shah, 1973). Ray methods enjoyed an increasing popularity in the seventies because, as they were computationally cheap, seismologists could use them to investigate 3-D inhomogeneous media (Cerveny et al., 1977; Cerveny and Hron, 1980). A few years ago, studies on seismic tomography boosted the development of fast seismic ray-tracing methods essentially aimed at computing traveltimes. Different ray-tracing algorithms, designed as a part of tomographic procedures, were presented for the two-dimensional case (Keller and Perozzi, 1983; Langan et al., 1985; Bishop et al., 1985) but fewer investigated a three-dimensional medium (Stöckli, 1984).

In this paper I present a fast seismic ray-tracing algorithm inspired by the work of J. Fawcett (1983), which can be applied to model seismic reflection surveys in

a three-dimensional layered medium. The algorithm can handle several seismic profiles and can be applied to different processing methods such as tomography and Kirchhoff migration; or it can be used as a tool to assist traveltime picking in complicated geological zones. In a second part of the paper, I develop the application of the ray-tracing to a 3-D tomographic procedure. The combined ray-tracing and inversion algorithms have been applied to a synthetic geological model in order to demonstrate the method's ability to recover 3-D structures using only traveltime information.

THE RAY-TRACING ALGORITHM

Ray-tracing environment

The ray-tracing algorithm is about the same, no matter which of the common-shot, common-receiver or common-midpoint gathers we want to model. As shown later, the main difference between the three of them is only a matter of choosing the appropriate continuation variables to derive a new ray from a neighboring one rapidly. In this paper I refer only to the CMP gather, a convenient domain for the tomographic procedure. Figure 1 demonstrates that rays propagate in a three-dimensional geological domain consisting of a number of arbitrarily shaped horizons which subdivide the earth into layers having some constant attributes. In the case examined, the only attribute of a layer is its wave propagation velocity, (usually P-wave velocity). The preliminary work that I present here assumes that this velocity is constant in all directions. The "velocity profile" can later be extended to a function of x and y $(v(x,y))$ and even perhaps to a function of x, y and depth $(v(x,y,z))$.

The parameterization of the horizons, $h_k(x,y), k = 1$ to *number of horizons*, requires a two-dimensional interpolator. The interpolator needs to be *reliable* with respect to precise depth informations provided by the interpreter, for instance from borehole data. It should also be sufficiently *smooth* to avoid local oscillations that certainly would alter the ray-tracing procedure. In the case of an application to tomography, the interpolator needs to be built on a set of consistent variables leading to a stable inversion process. From my experience with 2-D VSP tomography (Guiziou et al., SEP-51), I would think that an interpolator based on B-splines (Dierckx, 1975, Inoue, 1986) should be fairly suitable. However, I have not yet found the most appropriate one and this point will require some future thought. The interpolator I currently do use is proposed by Inoue (1986), and is built on a regular grid of B-splines functions of degree 3.

The ray-tracing algorithm can handle an arbitrary number of seismic lines located on the surface of the earth. These lines are independent from one another and represent the successive locations of the common-midpoints that we want to model. The geometric attributes such as the number of midpoints, the distance

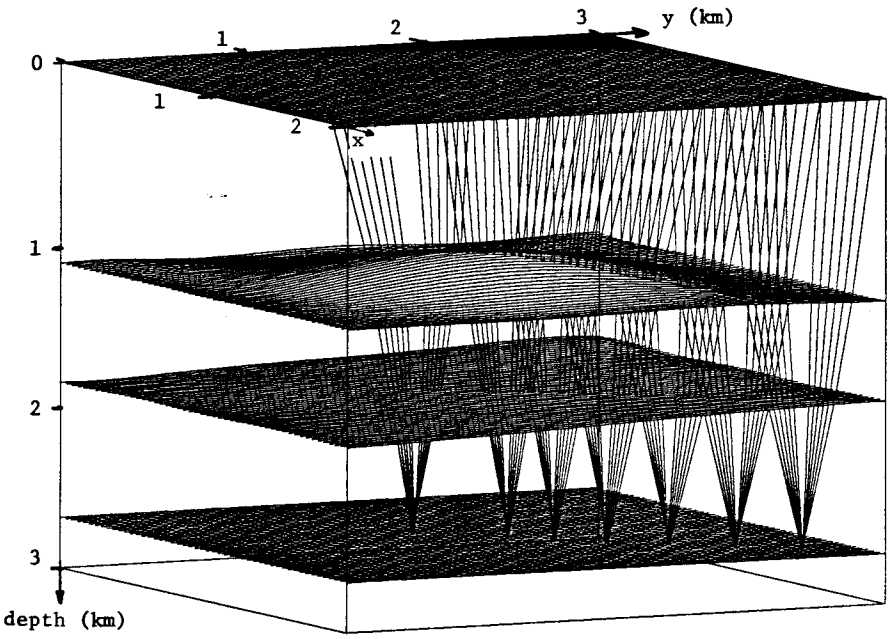

FIG. 1. Ray-tracing geometry. The three-dimensional model consists in homogeneous layers separated by arbitrarily shaped horizons. The small dots on the surface depict the seismic line. This simple example involves only seven common-midpoints with six offsets. Here the earth surface is assumed to be horizontal but there is no restriction to model an arbitrary topography.

between two of them, the number of offsets, etc., can vary from one line to another. This enables easier linking between the traveltimes computed by ray-tracing and the traveltimes actually measured on the field.

The computation of a raypath

The basics for raypath computation is similar to the one proposed for the 2-D VSP tomography (Guiziou et al., SEP-51). We want to compute the raypath between two points on the earth that are identified as the source and receiver locations. As seen in Figure 2, the ray issued from the source propagates through a number of layers, reflects on a given horizon, and eventually reaches the receiver. The difference between the broken line generated by the raypath and any other broken line that reflects on the same horizon linking the source and the receiver is that the former optimizes the traveltime through the earth (Fermat's principle). Hence, given a source location, a receiver location and a reflecting horizon, we compute the raypath as the broken line satisfying Fermat's principle.

Let us consider a ray crossing $N+1$ layers. The traveltime of this ray can be expressed as:

$$t = \sum_{i=1}^{N+1} t_i = \sum_{i=1}^{N+1} \frac{D_i}{V_i}$$

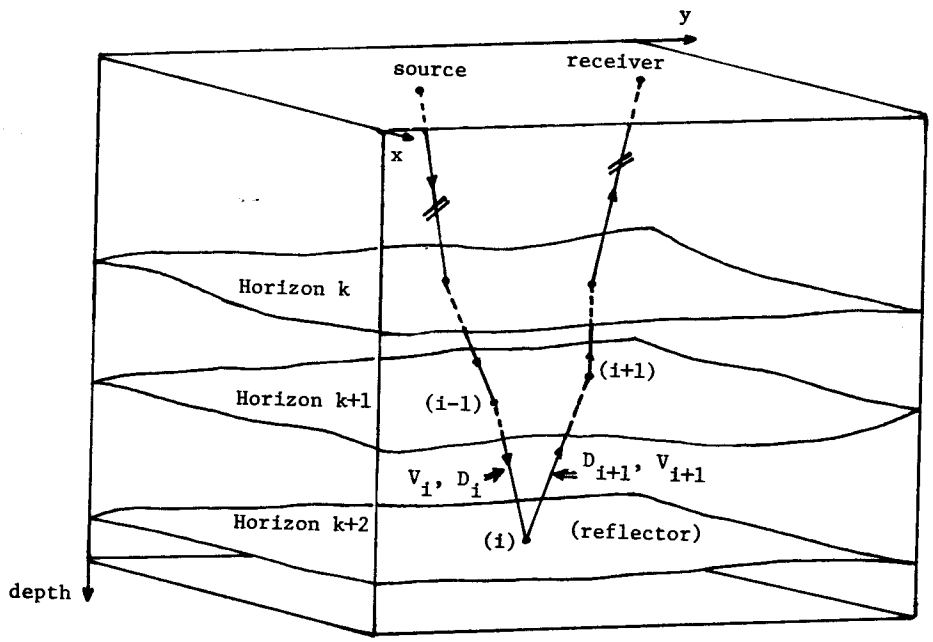

FIG. 2. Computation of the optimal raypath between the shot and the geophone. The reflector is known. The unknowns are the intersection points between the ray and the horizons.

where $D_i = \left[(x_i - x_{i-1})^2 + (y_i - y_{i-1})^2 + (z_i - z_{i-1})^2\right]^{1/2}$ measures the length of the $i-th$ segment of the ray, and V_i is the wave propagation velocity in the layer crossed by this segment.

We compute the location of the successive intersection points between the ray and the horizons by stating that:

$$\frac{\partial t}{\partial X} = 0,$$

where $X = (x_1, y_1, x_2, y_2, ..., x_N, y_N)$ represents the vector of our $2N$ unknowns (x_i, y_i).

This leads to a non-linear system of $2N$ equations in $2N$ unknowns, $\Phi = \begin{bmatrix} \phi_1 \\ \phi_2 \\ . \\ . \\ \phi_{2N} \end{bmatrix}$

with

$$\begin{cases} \phi_{2i-1} = \frac{\partial t_i}{\partial x_i} + \frac{\partial t_{i+1}}{\partial x_i} = 0 \\ \phi_{2i} = \frac{\partial t_i}{\partial y_i} + \frac{\partial t_{i+1}}{\partial y_i} = 0 \, ; \end{cases}$$

that is,

$$\begin{cases} \phi_{2i-1} = \frac{1}{V_i}\left[\frac{\partial D_i}{\partial x_i} + \frac{\partial D_i}{\partial z_i}.\frac{\partial z_i}{\partial x_i}\right] + \frac{1}{v_{i+1}}\left[\frac{\partial D_{i+1}}{\partial x_i} + \frac{\partial D_{i+1}}{\partial z_i}.\frac{\partial z_i}{\partial x_i}\right] = 0 \\ \phi_{2i} = \frac{1}{V_i}\left[\frac{\partial D_i}{\partial y_i} + \frac{\partial D_i}{\partial z_i}.\frac{\partial z_i}{\partial y_i}\right] + \frac{1}{v_{i+1}}\left[\frac{\partial D_{i+1}}{\partial y_i} + \frac{\partial D_{i+1}}{\partial z_i}.\frac{\partial z_i}{\partial y_i}\right] = 0 . \end{cases}$$

This system $\Phi(X) = 0$ will be solved by an iterative Newton method:

$$\Phi\left(X^\nu + \delta X^\nu\right) = \Phi\left(X^\nu\right) + \delta X^\nu . \frac{\partial \phi\left(X^\nu\right)}{\partial X^\nu} = 0 \qquad (1)$$

where $J = \frac{\partial \phi(X^\nu)}{\partial X^\nu}$ is the matrix of the partial derivatives of the "error" functions $\phi_k()$, with respect to the components of X. This Jacobian matrix turns out to be seven-diagonal; we use an $L - U$ factorization algorithm to solve equation (1).

The initial solution X^0 required by the Newton algorithm is obtained by using continuation techniques. The paper on 2-D VSP tomography (SEP-51) provides a description of the continuation. If a field profile is to be modeled, the continuation should be applied to the location of the receivers. If a common-receiver gather is to be traced, then continuation should be applied on the shot locations. In the case of the CMP gather discussed here, we apply the continuation on the shot and receiver locations simultaneously.

APPLICATION TO TOMOGRAPHY

The ray-tracing algorithm can be used to derive an image of the local subsurface by using a tomographic procedure. To do this, we must dispose of a data set of recorded traveltimes from different lines of seismic reflection experiments conducted in a given area. The ray-tracing is now *data − driven*, because we compute only the rays that correspond to the geometric attributes (position of common-midpoints, number of offsets, etc.) of the traveltimes that have been picked on the seismic sections. In the case of 3-D surface-collected data, the picking of the traveltimes can be very difficult. I will not investigate the issue here; this is not a trivial problem. The tomographic approach consists of perturbing an initial guess of the geological model so as to find an optimal fit between the observed and computed traveltimes. In this section of the paper, I emphasize the link between the modeling and inversion procedures, and present the inversion algorithm used to perturb the geological model.

What can we expect from tomography?

One of the major difficulties in 3-D tomography arises from the fact that we want to optimize a set of rectangular grids of variables defining the horizons, and later, the velocities, by using data mainly distributed along lines (e.g. CMP lines). We are likely to encounter a situation where only a subset of the variables will be involved

in the inversion. Remaining variables might perturb the shape of the horizons after inversion. At this point, a good interpolator might be helpful, as it could attenuate the discrepancy between the two classes of variables. If we apply tomography on a single line of common-midpoints, can we reasonably expect a valid estimate of the geological model in the off-line direction? The proper model to consider in this case seems to be a cylindrical one with a constant dip across the line.

A second limitation of reflection tomography is that we usually want to solve for the velocity field and for the spatial position of the reflectors by using only one class of rays: the reflected ones. We do not have the combination of transmitted and reflected arrivals, as in VSP tomography, to help and discriminate between the velocity and reflectors parts. As we shall see in the synthetic examples, avoiding too many equivalences in a simultaneous inversion of several horizons and layer velocities requires that the database refers to different reflectors located at different depths so that the geological model can be recovered in depth progressively, as the inversion iterations proceed. A good alternative is to exploit any available seismic data recorded in boreholes that might be located in the area of interest.

Getting a reliable image of the earth requires that we know, for a given CMP, where the different common-depth points are actually located on the reflector. If this can be reasonably estimated in the in-line direction by measuring the ray parameter (or gradient in time $p = \frac{\partial t}{\partial x}$) on zero-offset or near-offset sections, it is more difficult for the off-line direction, even if we have several lines. The solution to get enough information in the off-line direction could be to interpolate the data between the lines if they are sufficiently close to each other.

The computation of the Jacobian for the inverse problem

Optimizing the model variables on the basis of a misfit between the observed and computed traveltimes demands assessment of the influence of each variable on the different traveltimes. That is, we need to compute the Jacobian vector $J = \frac{\partial t}{\partial P}$, where t is a traveltime, and P the vector of variables.

Recall that the traveltime of a given ray can be written as:

$$t(X,Y,Z,V) = \sum_{i=1}^{N+1} \frac{D_i(x_{i-1}, x_i, y_{i-1}, y_i, z_{i-1}, z_i)}{V_i}.$$

In this particular case of constant velocities in layers, the partial derivative of t with respect to a velocity V_i is obviously:

$$\frac{\partial t}{\partial V_i} = -\frac{D_i}{(V_i)^2}.$$

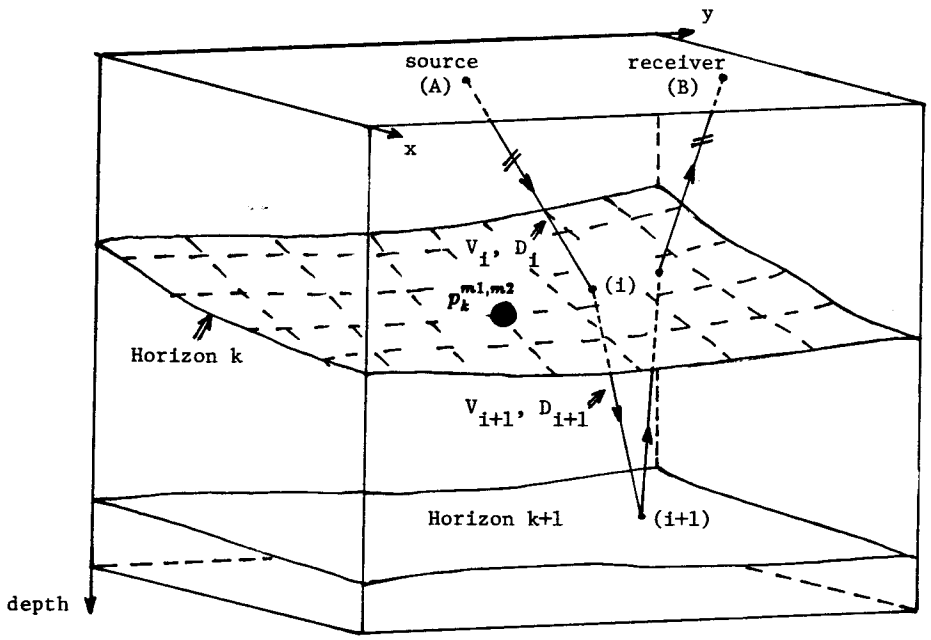

FIG. 3. Computation of the influence of a given horizon variable on the traveltime of the ray. Because the interpolator is defined by **local** B-splines, only a few variables surrounding the intersection points are involved.

The determination of the partial derivatives of t with respect to horizon variables requires more analysis. Let me refer to Figure 3 in which I consider a given variable, $p_k^{m1,m2}$, on the horizon k. The influence of this variable on the traveltime t of the ray AB can be derived as follows:

$$\frac{\partial t}{\partial p_k^{m1,m2}} = \sum_{i=1}^{N+1} \frac{1}{V_i} \cdot \frac{\partial D_i(x_{i-1}, x_i, y_{i-1}, y_i, z_{i-1}, z_i)}{\partial p_k^{m1,m2}}, \tag{2}$$

with

$$\frac{\partial D_i}{\partial p_k^{m1,m2}} = \frac{\partial D_i}{\partial x_{i-1}} \cdot \frac{\partial x_{i-1}}{\partial p_k^{m1,m2}} + \frac{\partial D_i}{\partial x_i} \cdot \frac{\partial x_i}{\partial p_k^{m1,m2}} + \frac{\partial D_i}{\partial y_{i-1}} \cdot \frac{\partial y_{i-1}}{\partial p_k^{m1,m2}} + \frac{\partial D_i}{\partial y_i} \cdot \frac{\partial y_i}{\partial p_k^{m1,m2}}$$

$$+ \frac{\partial D_i}{\partial z_{i-1}} \cdot \frac{\partial z_{i-1}}{\partial p_k^{m1,m2}} + \frac{\partial D_i}{\partial z_i} \cdot \frac{\partial z_i}{\partial p_k^{m1,m2}}.$$

Notice that for $i = 1$ and $i = N+1$ we come up with the entities $\frac{\partial D_1}{\partial x_0}$, $\frac{\partial D_1}{\partial y_0}$, $\frac{\partial D_1}{\partial z_0}$, $\frac{\partial D_{N+1}}{\partial x_{N+1}}$, $\frac{\partial D_{N+1}}{\partial y_{N+1}}$ and $\frac{\partial D_{N+1}}{\partial z_{N+1}}$ which are equal to zero because the points (x_0, y_0, z_0) and $(x_{N+1}, y_{N+1}, z_{N+1})$ correspond respectively to the source and the receiver, which are known to be constant. Taking this into account, we can now re-index the summation of equation (2) and transform it into:

$$\frac{\partial t}{\partial p_k^{m1,m2}} = \sum_{i=1}^{N} \left\{ \left(\frac{1}{V_i} \cdot \frac{\partial D_i}{\partial x_i} + \frac{1}{V_{i+1}} \cdot \frac{\partial D_{i+1}}{\partial x_i} \right) \frac{\partial x_i}{\partial p_k^{m1,m2}} + \left(\frac{1}{V_i} \cdot \frac{\partial D_i}{\partial y_i} + \frac{1}{V_{i+1}} \cdot \frac{\partial D_{i+1}}{\partial y_i} \right) \frac{\partial y_i}{\partial p_k^{m1,m2}} \right\}$$

$$+ \sum_{i=1}^{N} \left(\frac{1}{V_i} \cdot \frac{\partial D_i}{\partial z_i} + \frac{1}{V_{i+1}} \cdot \frac{\partial D_{i+1}}{\partial z_i} \right) \frac{\partial z_i}{\partial p_k^{m1,m2}}. \qquad (3)$$

Recognize now that the first summation of equation (3) applies to a term in brackets that exactly states Fermat's principle. This first summation cancels, and we end up with the equation

$$\frac{\partial t}{\partial p_k^{m1,m2}} = \sum_{i=1}^{N} \left(\frac{1}{V_i} \cdot \frac{\partial D_i}{\partial z_i} + \frac{1}{V_{i+1}} \cdot \frac{\partial D_{i+1}}{\partial z_i} \right) \frac{\partial z_i}{\partial p_k^{m1,m2}}. \qquad (4)$$

An interesting point to notice is that only the term $\frac{\partial z_i}{\partial p_k^{m1,m2}}$ depends on the interpolator used to represent the horizons. The computation of this Jacobian vector is efficient because the term enclosed in parentheses in equation (4) is a "by-product" of the raypath computation.

Updating the geological model

We have derived methods to model traveltimes and to measure the influence of the model variables on those traveltimes. An inversion algorithm can now be used to perturb the geological model so as to optimally reduce the misfit between the computed and the observed data. Because we think of the geology in terms of depth horizons subdividing the earth into homogeneous layers, the variables to be inverted will be the entities that define the shape of the horizons and the value of the velocity within each layer. In the case described here, the horizons are built on a grid of knots on which the B-splines of degree 3 are defined. The inversion variables will be the coefficients associated with each knot of the grid. (Refer to Inoue for more details). These coefficients can be regarded as depth values, because the depth of the horizon at a given point is computed as a linear combination of a few surrounding knot coefficients.

The inversion algorithm proposed by Tarantola and Valette (1982), tackles the issue of multiple solutions by introducing probabilistic assumptions (Gaussian distribution) for the observed data and the model variables. This approach enables us to look for the maximum likelihood set of variables around some a priori position provided by the user. The model variables are updated by solving the system:

$$Hessian * (p_{k+1} - p_k) = -Gradient,$$

where

$$Hessian = G_k^T C_{d_0}^{-1} G_k + C_{p_0}^{-1}$$

$$Gradient = G_k^T C_{d_0}^{-1} (d_c - d_o) + C_{p_0}^{-1} (p_k - p_0);$$

with
p_0 : a priori set of variables,
p_k : set of variables at iteration k,
d_o : observed data,
d_c : computed data,
G_k : Jacobian matrix at iteration k,
C_{d_0} : covariance matrix on observed data, and
C_{p_0} : covariance matrix on model variables.
This algorithm is computationally efficient and leads to a fast convergence, provided that the a priori model is reasonable. Both the Hessian and the Gradient are built up in the same time as the seismic rays are computed. We thus do not need to store the Jacobian matrix, a matrix that could become very large if several seismic lines were inverted.

For this algorithm to work, the user needs to supply information on the global attributes of the geological model he expects (p_0); on the degree of freedom that he allows to the variables (C_{p_0}); and on the distribution of the errors in the data (C_{d_0}). The inversion result is not sensitive to small variations of these pieces of information. Nonetheless, it seems interesting to try to establish a set of *rules* leading to the most appropriate values for these parameters, depending on the data that we are studying. Up to now, the matrices C_{p_0} and C_{d_0} have been considered to be diagonal. This means that we think of the probabilistic aspect of the data and variables only in terms of variances. A look at the synthetic examples will show the range of variances that is suitable for a stable inversion. An obvious improvement would seem to be the integration of genuine covariance matrices in the inversion algorithm. However, such an integration would not be straightforward because, besides forcing an increased computational cost, it would require the study of adequate covariance models for the picked traveltimes and the geological variables.

SYNTHETIC EXAMPLES

The following figures present and comment upon a number of inversion tests. The tests were designed to study both the behavior of the algorithm in the presence of different parameters such as model variances; and to relate the quality of the result to the amount and the repartition of the information supplied by the database. All the examples have been run on the Convex C1; it should be noted that the tomographic procedure is entirely interactive. A complete run with two or three iterations does not exceed five minutes of real time.

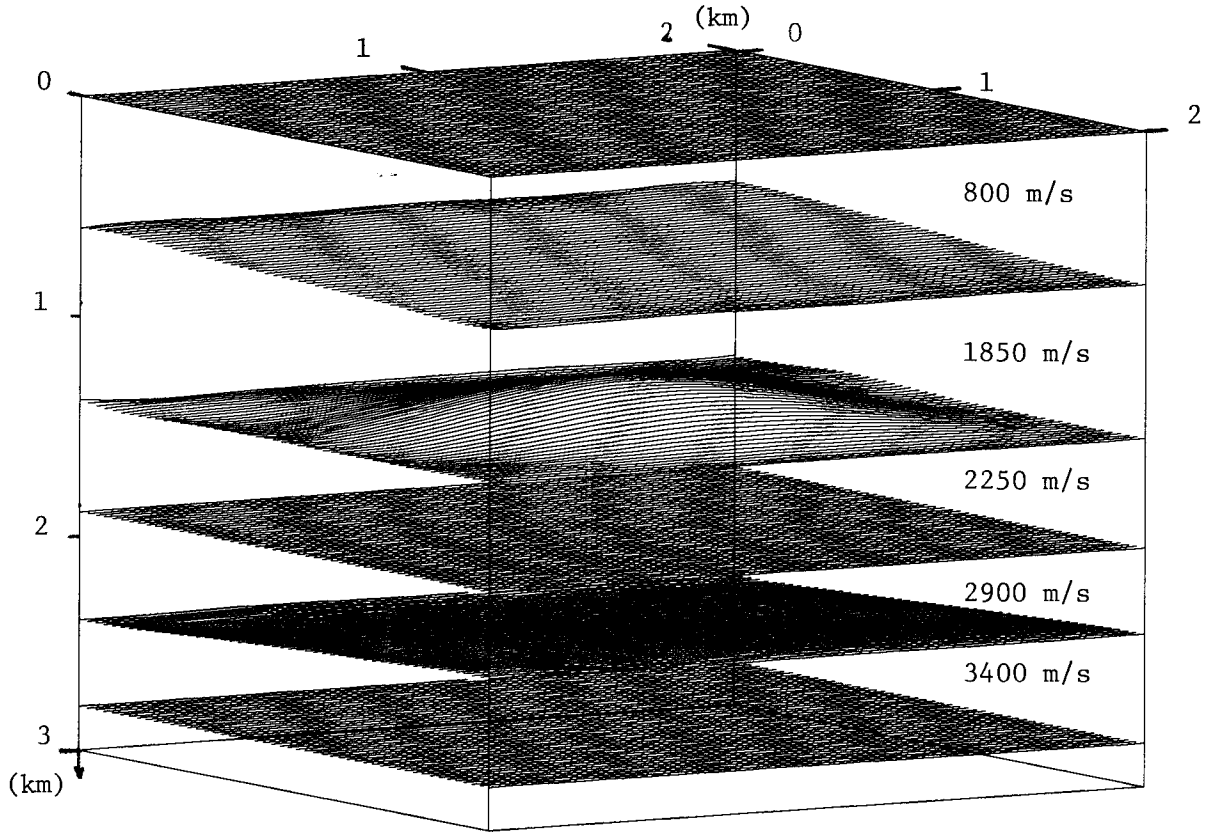

FIG. 4. The basic geological model used for the inversion tests following. The area of interest extends 2 kms both in X and Y directions; the subsurface is investigated down to a depth of 3 kms. The geology is modeled by five homogeneous layers separated by smoothly shaped horizons. The earth surface is supposed to be horizontal. Except for Horizons 1 and 4 which are dipping of 10% and 5% in opposite directions respectively, the main structural feature is a small anticline identified as Horizon 2.

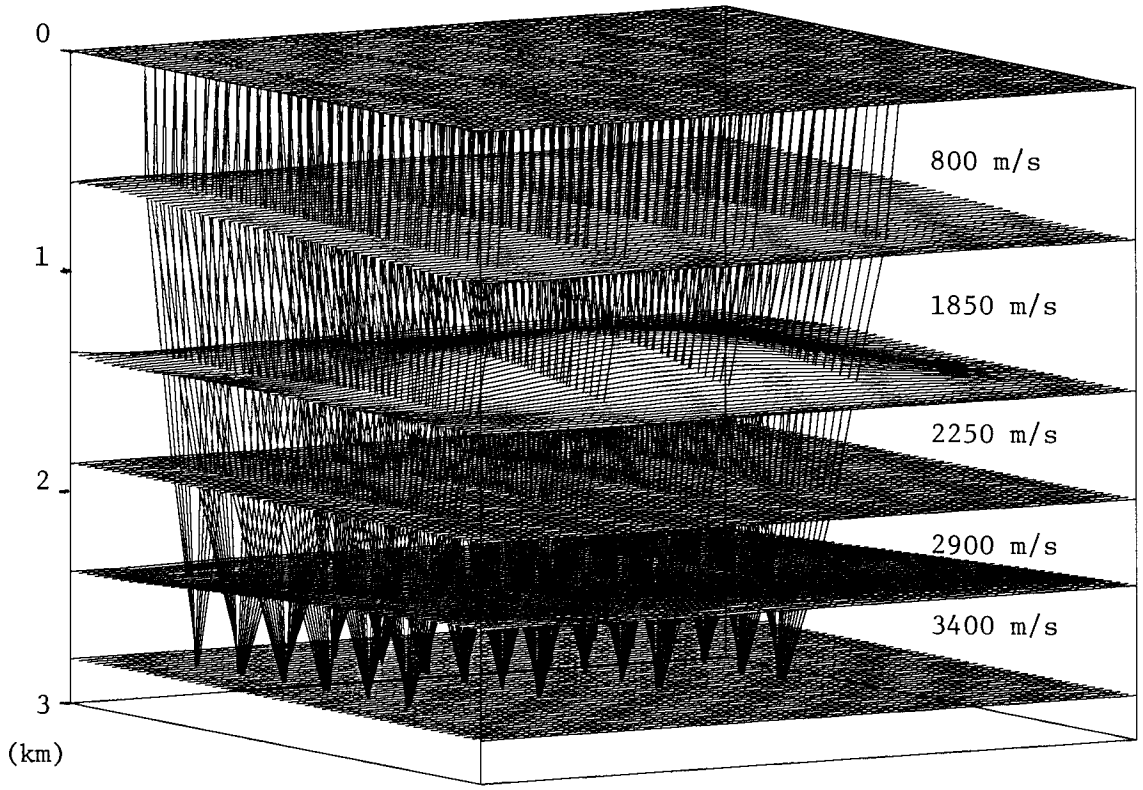

FIG. 5. The seismic survey is composed of four parallel lines located at 400 meters distances from each other. For each line, the data have been sorted on the basis of six common-midpoints with ten offsets ranging from 120 to 570 meters. The common-midpoints are located 200 meters apart from each other along the line. As we can see here, such a survey generates fairly good coverage of our geological volume, one suitable for tomography.

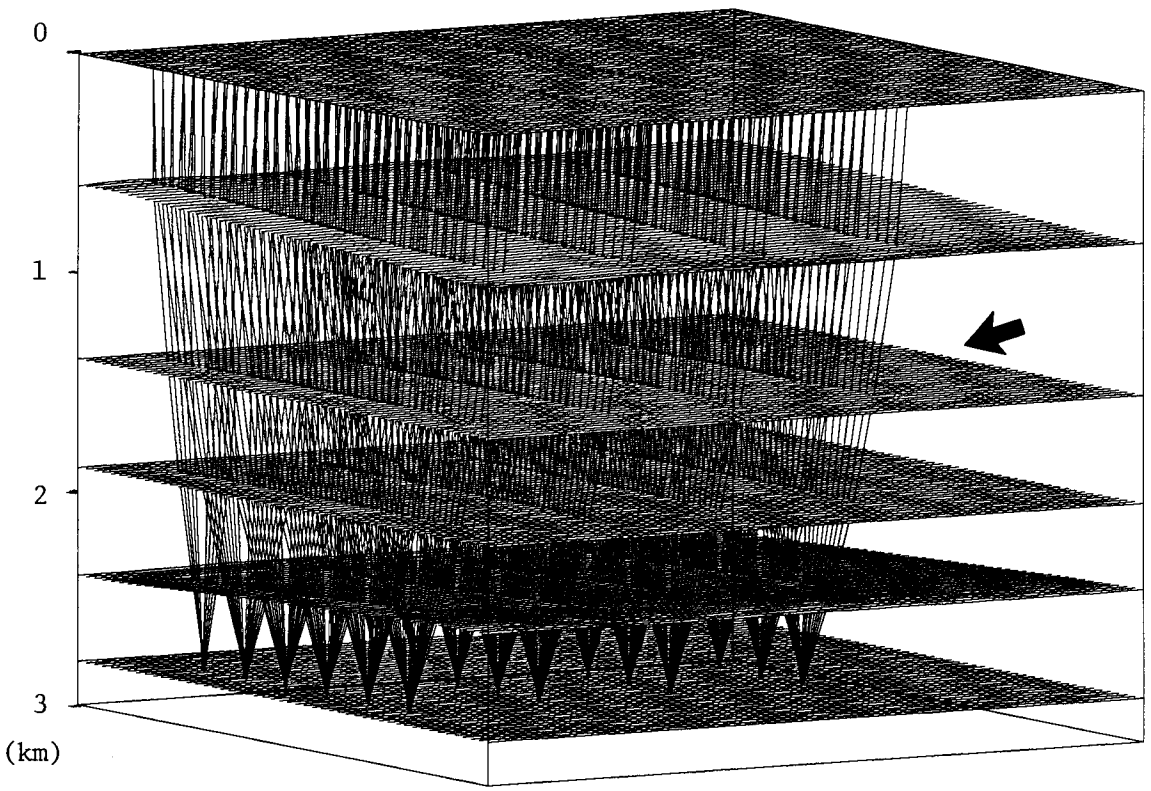

FIG. 6. Inversion 1. Using the four seismic lines and the rays reflected on Horizon 5, let us try to recover the anticline shape of Horizon 2. The initial guess for this horizon is horizontal. Only the velocities and the other horizons are supposed to be exactly known. We dispose of 216 reflected rays, and are inverting for 49 horizon parameters. The quadratic mean misfit between the computed and digitized traveltimes turns out to be 17 ms, a reasonable value.

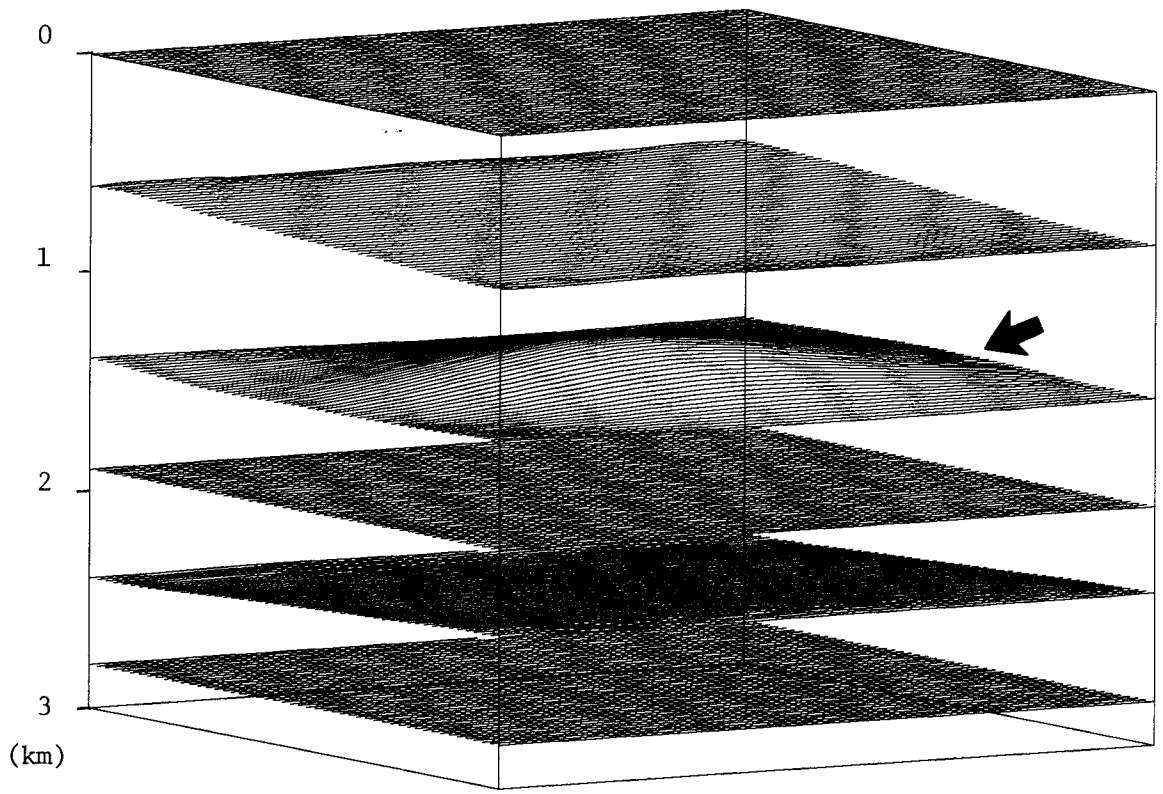

FIG. 7. Inversion 1. This result is obtained after the first iteration of the inversion. The variances have been set to 2 ms for the data (C_{d_0}), and to 100 meters for the unknown horizon (C_{p_0}). These parameters, in this case, seem adequate for obtaining a stable inversion. The quadratic mean misfit in traveltime has decreased to 0.63 ms. A second iteration, not shown here, confirms the recovery of the anticline and sets the misfit to 0.11 ms.

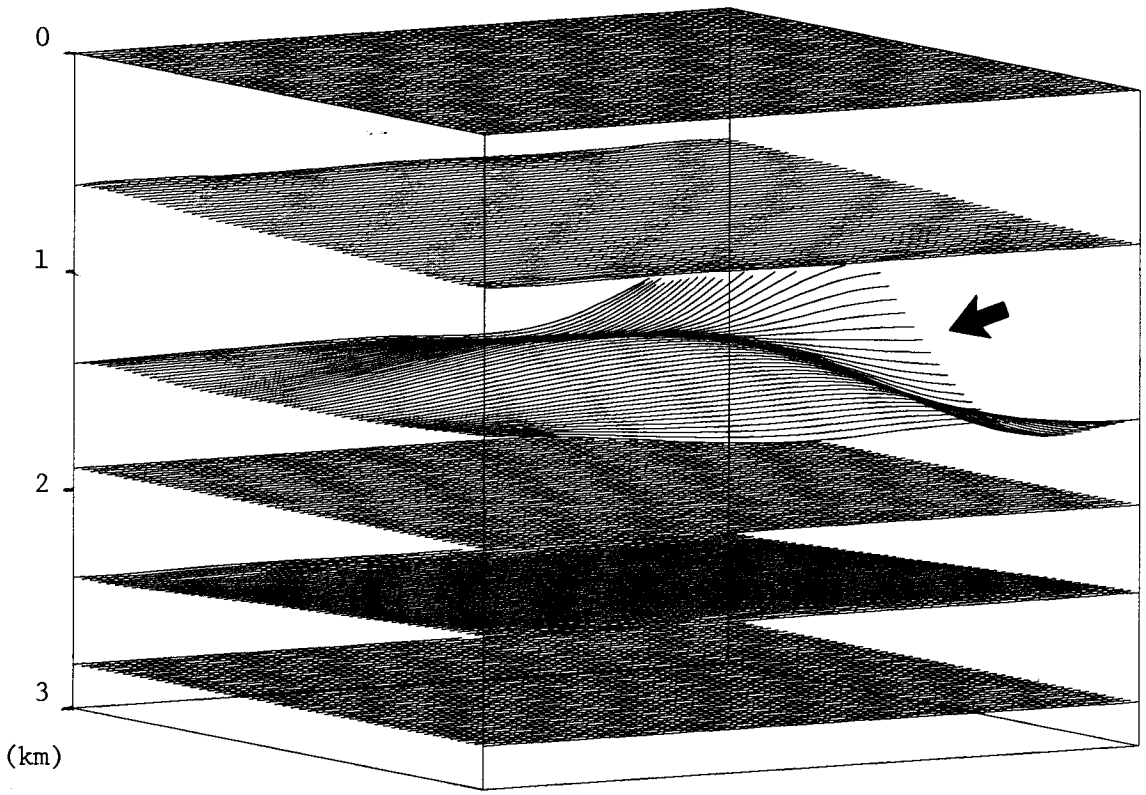

FIG. 8. Inversion 2. This is a test of the influence of the covariance C_{p_0} on the quality of the inversion. Here C_{p_0} has been set to 10000 meters, which gives full liberty to the inversion variables. A look at this figure shows that the variables tend to behave *randomly* in the right region, not illuminated by the rays. Tracing rays through this medium leads to a time misfit of 1.2 ms only: This confirms that the oscillating part of the horizon is hardly involved.

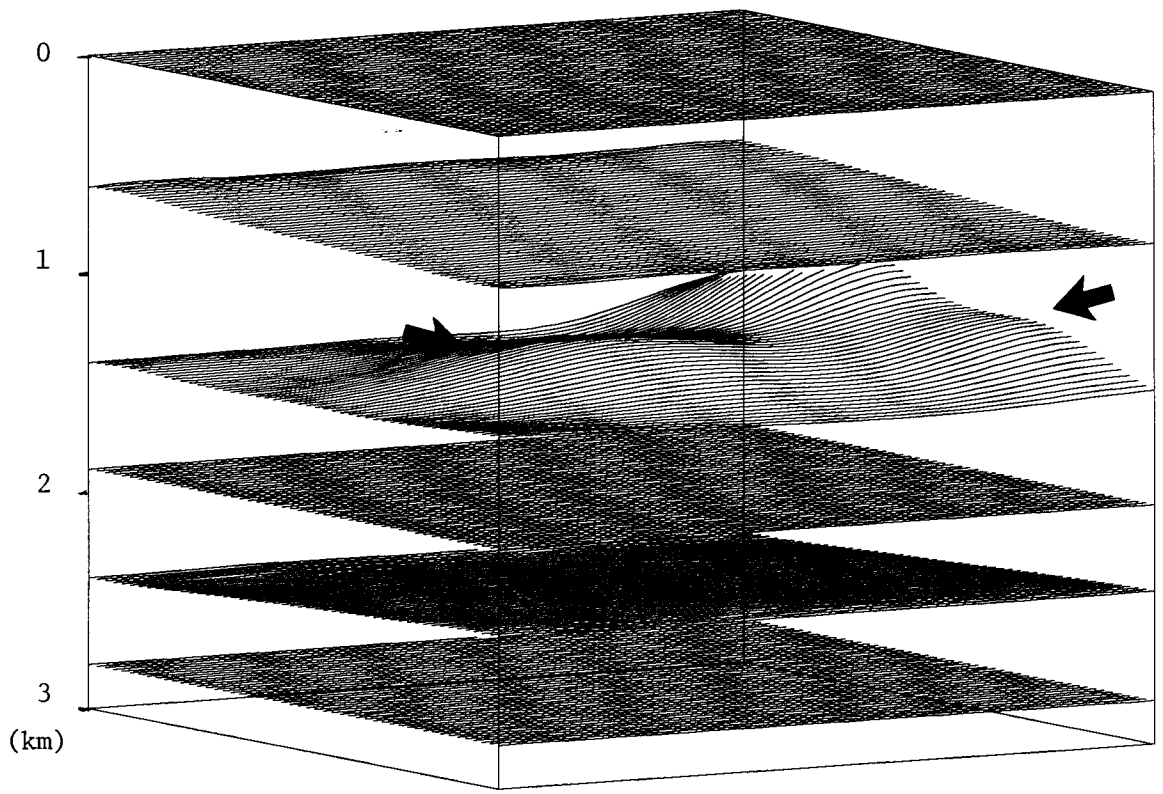

FIG. 9. Inversion 2. We are still studying the point where $C_{p_0} = 10000$ meters. Here is the result of the second iteration of inversion. Notice that the anticline emerges fairly well, and that the oscillations on the side are now attenuated. The time misfit has decreased to 0.33 ms.

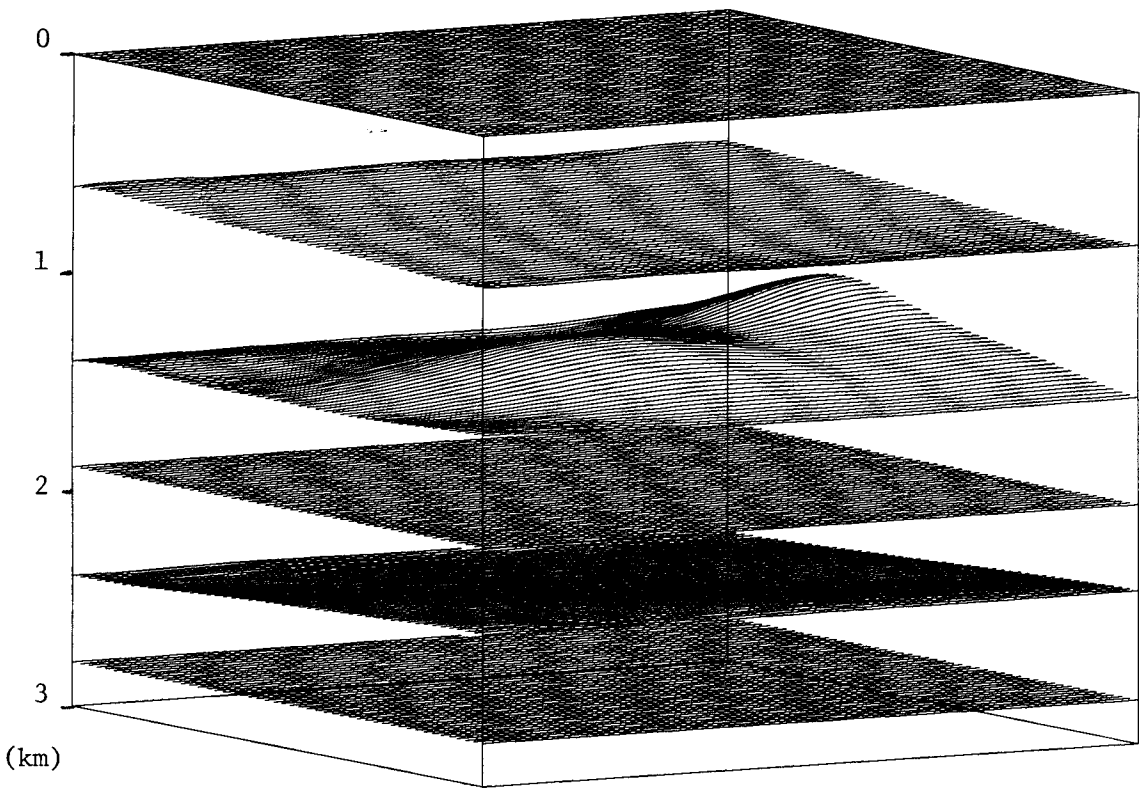

FIG. 10. Inversion 2. A quick look at the third iteration of this Inversion 2 confirms that the scheme will eventually converge to a reasonable solution in the region illuminated by the rays. The time misfit is now just 0.17 ms.

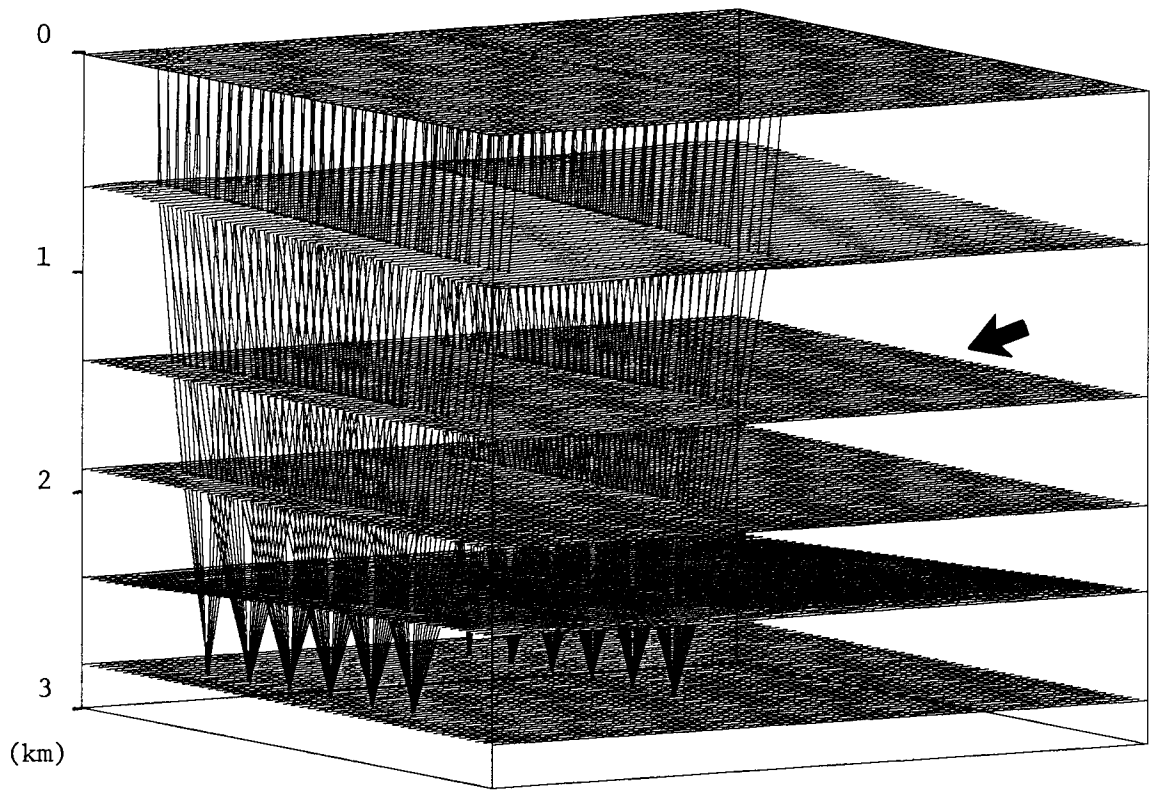

FIG. 11. Inversion 3. We are still examining the simple Horizon 2 inversion only. The available data is here reduced by a factor of two, working with the first and the third seismic lines only. The initial guess for Horizon 2 is unchanged with respect to Inversions 1 and 2; the initial time misfit is still 17 ms.

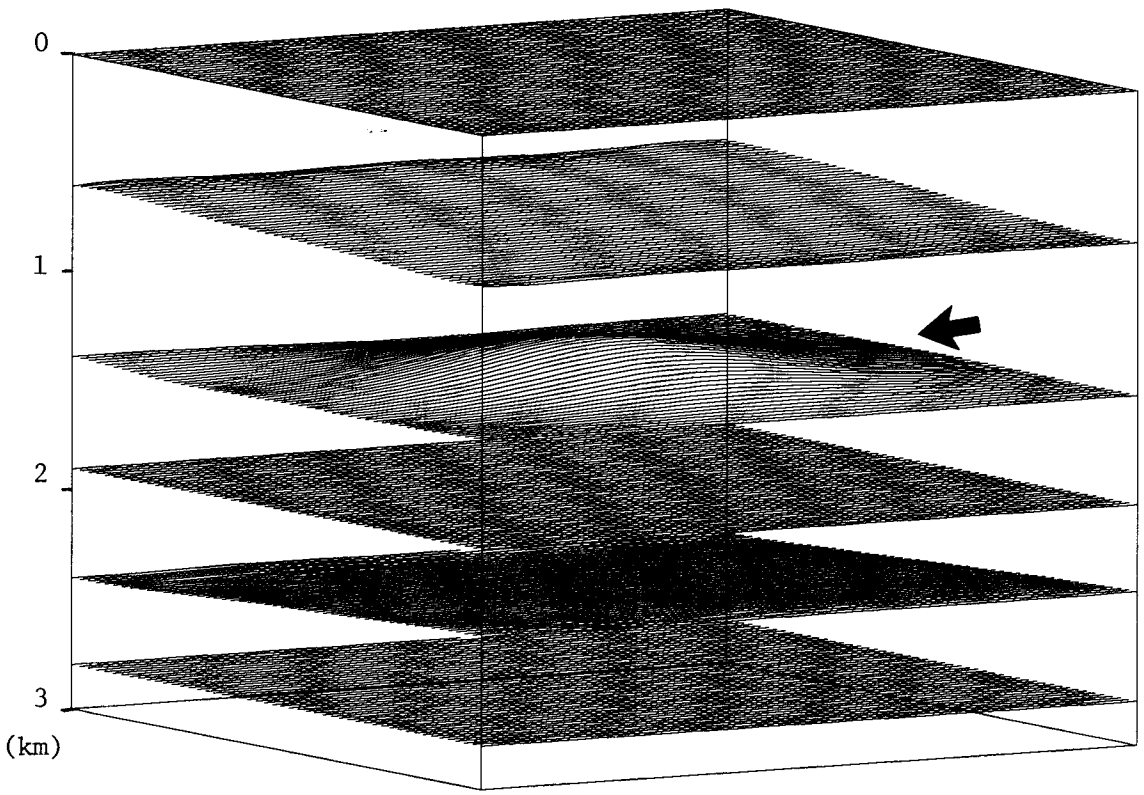

FIG. 12. Inversion 3. This figure shows that dropping off two seismic lines did not affect the result of the inversion. The 108 rays left are sufficient to constrain the 49 parameters. We are looking at the second iteration of the inversion for which $C_{p_0} = 100$ meters. The time misfit is down to 0.15 ms.

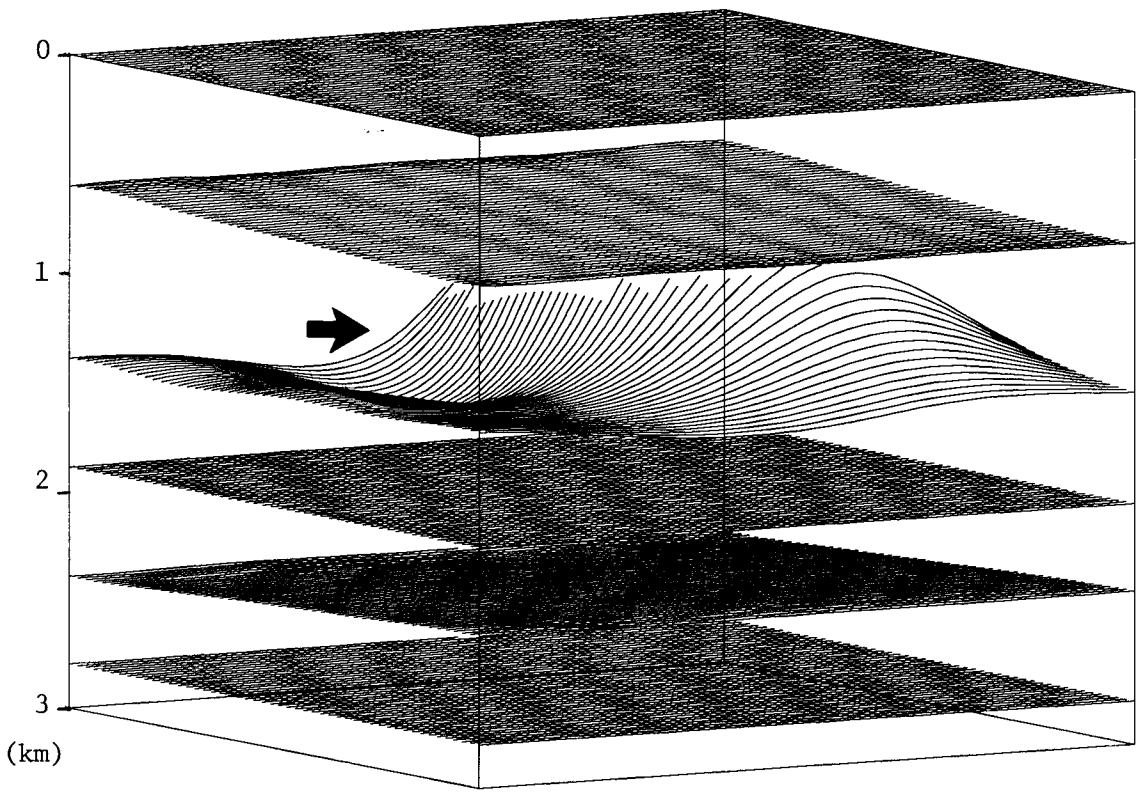

FIG. 13. Inversion 4. This figure notes the bad situation encountered at the first iteration of Inversion 3 where the covariance C_{p_0} is changed to 10000 meters. It is obvious here that just two seismic lines are insufficient to constrain such free parameters. The difference between Inversion 2 and this result tells us that the choice of C_{p_0} is important; this parameter definitely depends on the data that we use for the tomography.

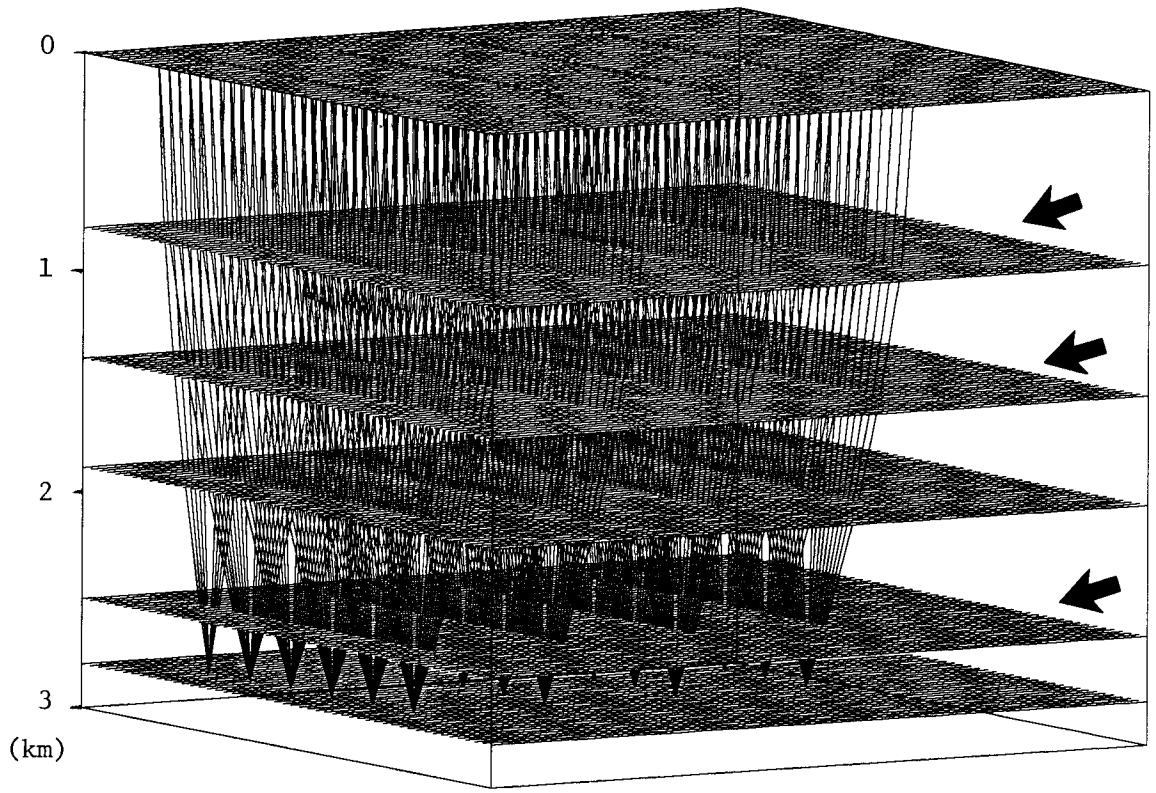

FIG. 14. Inversion 5. The inversion scheme is complicated here to attempt to invert for the three horizons 1,2 and 4; that is all but the horizontal ones. From now on, C_{d_0} will be set to 2 ms, and C_{p_0} to 100 meters. Again, here we use four seismic lines and only one reflector. As illustrated, the initial geological model is completely horizontal and the corresponding time misfit is 252 ms.

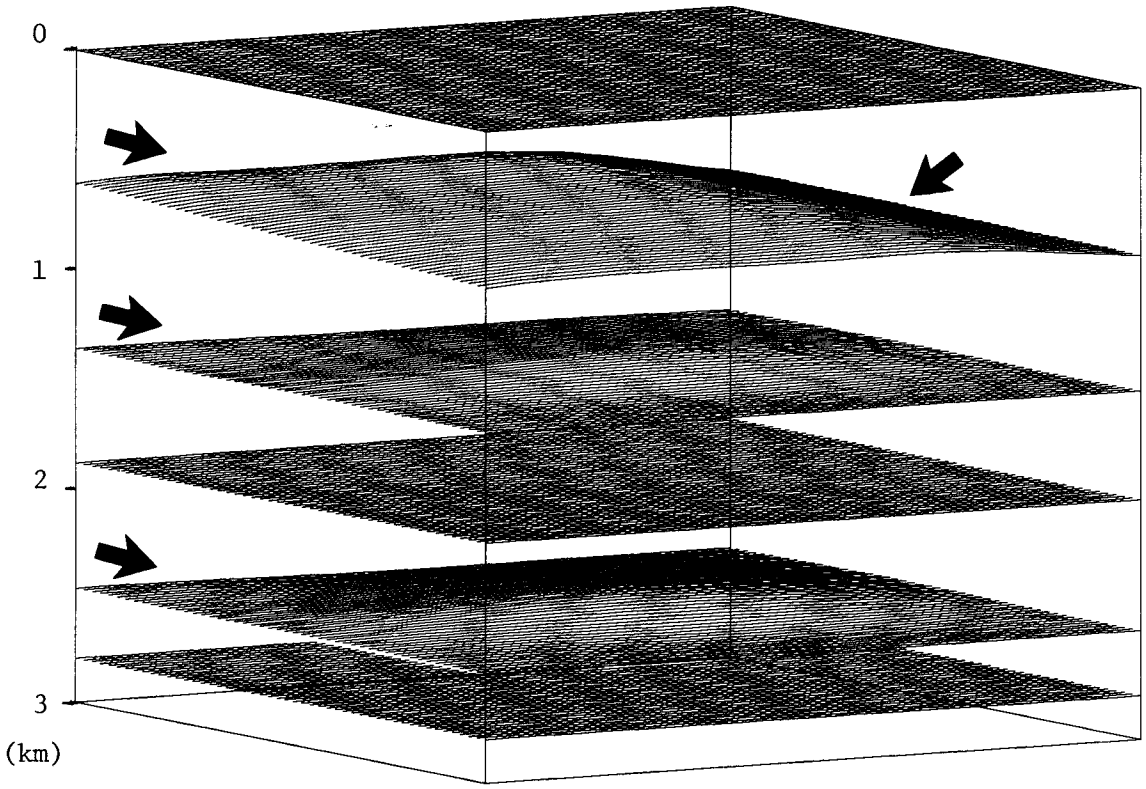

FIG. 15. Inversion 5. A second iteration result, an interesting illustration of the non-uniqueness of the inversion solution. We end up with a geological model which is significantly different from the expected one, yet the traveltime misfit is only 0.20 ms. In this case, we have 216 rays to invert for 147 parameters. There is obviously insufficient information to discriminate between the three unknown horizons. The small ratio of rays to parameters is not the major limiting factor, however; it is the fact that we use only one reflector. Notice also that the inversion of the first horizon is strongly dependent upon the spreading geometry of the rays: the right side is not illuminated, hence is poorly inverted.

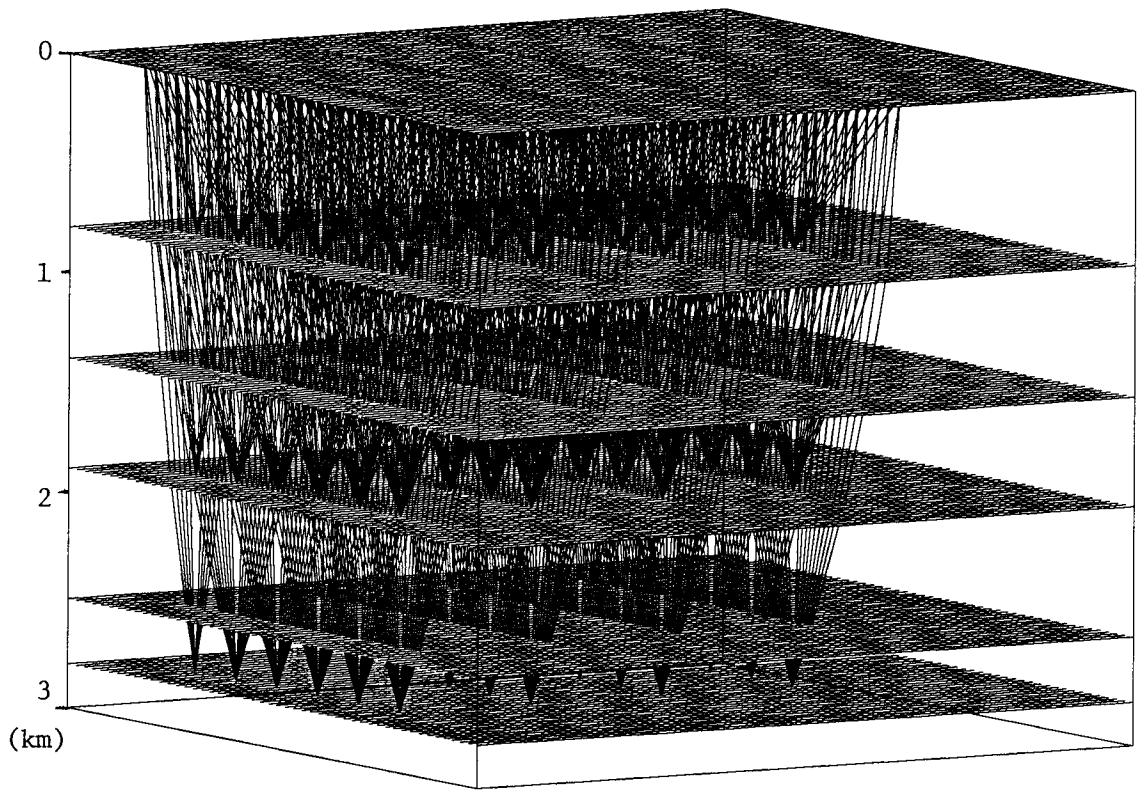

FIG. 16. Inversion 6. The last example demonstrated a need for more information. Accordingly, we shall again try to invert Horizons 1,2 and 4 but this time with a database referring to the rays that reflect on Horizons 1,3 and 5. More than an increased number of rays, it is an improvement in the repartition of the information which makes us expect a better result.

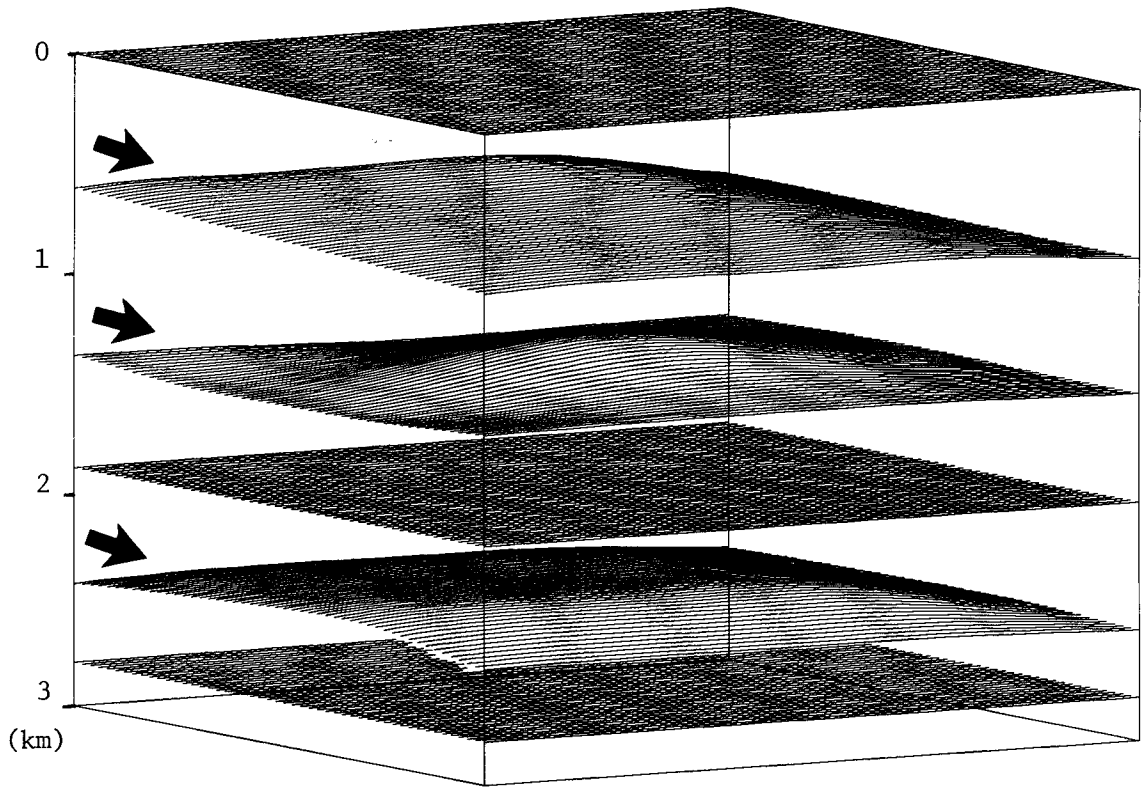

FIG. 17. Inversion 6. A second iteration of the inversion, demonstrating that the information contained in the database is now sufficient to discriminate between the three horizons. The result can be considered good, since the unknown horizons are fairly well-recovered within the area of influence of the rays. (Refer to previous figure for comparison). The quadratic mean time misfit was 252 ms for the initial model; after two iterations it dropped to 0.14 ms.

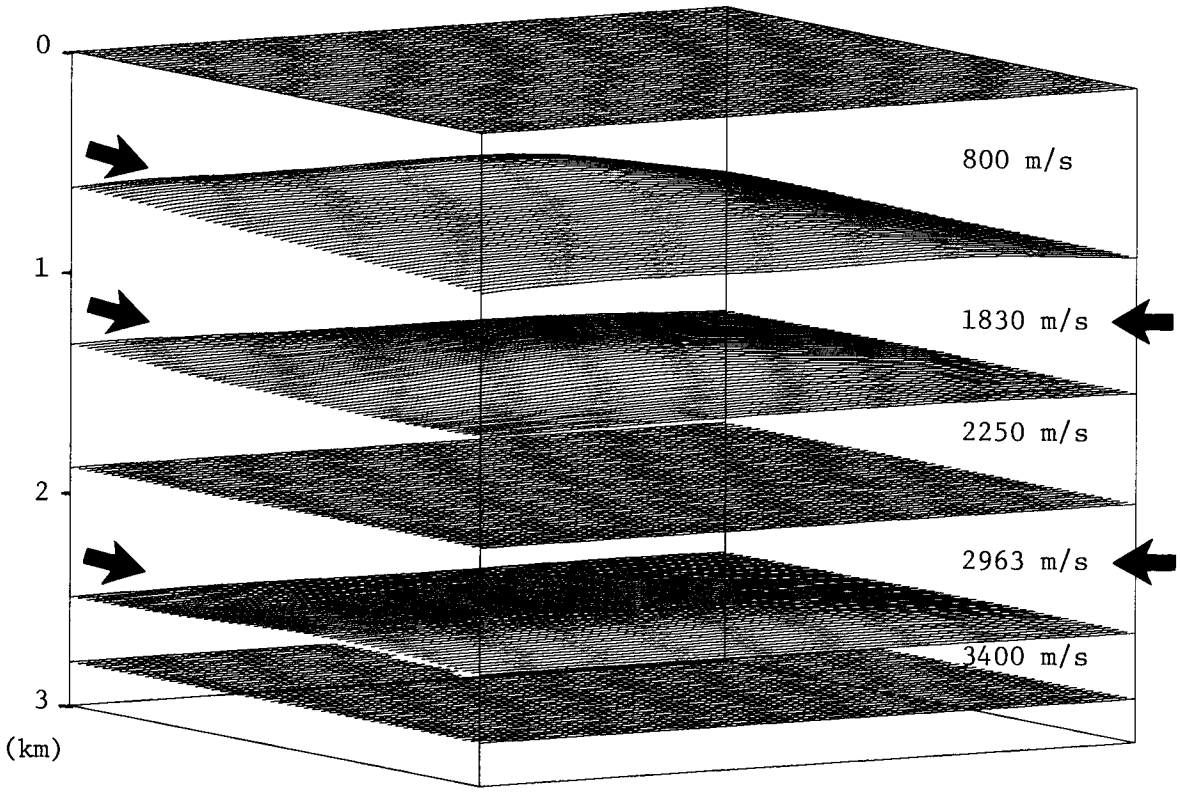

FIG. 18. Inversion 7. This last example studies the combined inversion of Horizons 1,2 and 4, and the two velocities in Layers 2 and 4. In this case, data from Reflectors 1,3 and 5 was used as in Inversion 6. We are looking at the result of the first iteration of the inversion, starting from a horizontally- layered medium for the horizons, and from velocities V2 = 1500 m/s (instead of a known velocity of 1850 m/s) and V4 = 2800 m/s (instead of 2900 m/s). The mean time misfit corresponding to the initial model was high -(394 ms). It has decreased drastically to 10 ms after this first iteration, however. The first horizon is properly inverted, as we could expect, but the two others are not yet very well recovered. This is due to the ambiguity between the unknown velocities and the unknown horizons. The velocity in the second layer is quite well recovered; this is not the case for velocity V4, in contrast.

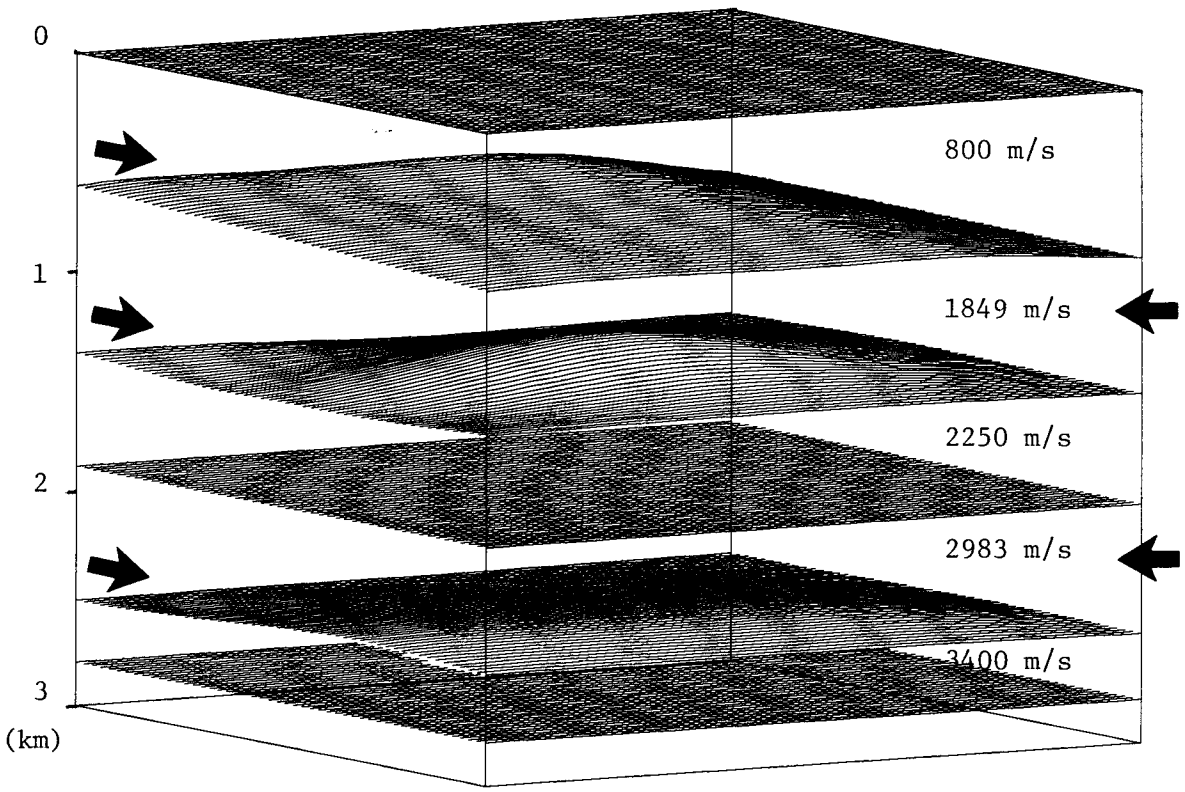

FIG. 19. Inversion 7. After three iterations, the tomographic procedure gives a fairly good result. It is interesting to note that the accuracy has propagated in depth while the iterations were proceeding. We end up with a good image of Horizons 1 and 2, and with an accurate velocity in Layer 2. The deepest targets are still not as well-resolved, especially the velocity in Layer 4. This can be understood if we think of rays decreasing in number as depth increases.

Discussion

Some simple examples demonstrate that we can expect interesting results from the traveltime inversion method, provided that a few important conditions are met: First, the choice of inversion parameters -covariances or variances- should be related to the expected quality and density of the data. If the interpreter thinks that the digitized traveltimes provide a good coverage of the area of interest, then the degree of freedom assigned to the variables to be inverted can be high. Conversely, sparse data or complicated geological structures require a more constrained subsurface model. Secondly, the geometry of the survey is an important parameter which directly affects the quality of the inversion. It seems obvious that many seismic lines, not necessarily parallel, should lead to the best result. A third important point made clear through the examples presented, is that reflection tomography requires data related to more than one reflector as soon as we want to invert for several horizons and layer velocities. If the latter condition is met, then the inversion scheme can recover the geology in depth as the iterations proceed.

CONCLUSIONS

This paper presented a general purpose two-point ray-tracing algorithm, in a three-dimensional layered medium, which has been applied to a specific data processing procedure: tomography. The ray-tracing algorithm has been derived to provide a fast and accurate computation of traveltimes in the case of reflection seismology. As demonstrated here for traveltime inversion, the analytical formulation of the ray-tracing leads to an easy and accurate link with another seismic procedure. The paper also showed that we can use traveltime inversion as a computationally cheap tool to investigate for three-dimensional structures in a given area. The work presented here can be extended to a more general parameterization of the geological medium, especially by introducing more sophisticated velocity functions in the layers.

REFERENCES

Bishop T. N., Bube, K. P., Cutler, R. T., Langan, R. T., Love, P. L., Resnik, J. R., Shuey, R. T., Spindler, D. A., Wyld, H. W., 1985, Tomographic determination of velocity and depth in laterally varying media: Geophysics, **50**, 903-923.

Cerveny, V. and Hron, F., 1980, The ray series method and dynamic ray-tracing system for three-dimensional inhomogeneous media: Bull. of the Seismological Society of America, **70**, No. 1, 47-77.

Cerveny, V., Molotkov, I. A., Psencik, I., 1977, Ray method in seismology: Charles Univ. Press, Prague.

Dierckx, P., 1975, An algorithm for smoothing, differentiation and integration of experimental data using splines functions: J. Comp. Appl. Maths 1, 165-184.

Fawcett, J. A., 1983, Three-dimensional ray-tracing and ray-inversion in layered media: PhD thesis, California Institute of Technology.

Guiziou, J. L., Dezard, Y. and Martayan, G., 1987, 2-D tomography for VSP: SEP-51.

Inoue, H., 1986, A least-squares smooth fitting for irregularly spaced data: Finite-element approach using the cubic B-splines basis: Geophysics, **51**, 2051-2066.

Keller, H. B. and Perozzi, D. J., 1983, Fast seismic ray-tracing: SIAM, **43**, No. 4.

Langan, R. T., Lerche, I. and Cutler, R. T., 1985, Tracing of rays through heterogeneous media: An accurate and efficient procedure: Geophysics, **50**, 1456-1465.

Shah, P. M., 1973, Ray-tracing in three dimensions: Geophysics, **38**, 600-604.

Stöckli, R. F., 1984, Two-point ray tracing in a three-dimensional medium consisting of homogeneous nonisotropic layers separated by plane interfaces: Geophysics, **49**, 767-770.

Tarantola, A. and Valette, B., 1982, Generalized non-linear inverse problems solved using the least square criterion: Rev. Geophys. Space Phys., **20**, 219-232.

Migration by Hypergeometric Transform